PHYSICAL REVIEW B **111**, 174102 (2025)

Phonon-driven mechanism for the chiral phase transition of K_3NiO_2

Mauro Fava,[1] Emma McCabe,[2] Aldo H. Romero,[3] and Eric Bousquet[1]
[1] *Physique Théorique des Matériaux, QMAT, Université de Liège, B-4000 Sart-Tilman, Belgium*
[2] *Department of Physics, Durham University, South Road, Durham DH1 3LE, United Kingdom*
[3] *Department of Physics and Astronomy, West Virginia University, Morgantown, West Virginia 26505-6315, USA*

(Received 21 May 2024; revised 26 March 2025; accepted 22 April 2025; published 6 May 2025)

We investigate the experimentally observed achiral-to-chiral displacive phase transition of K_3NiO_2 using first-principles calculations. Phonon dispersion analysis of the achiral phase reveals the presence of an unstable phonon branch, with the low-symmetry chiral phases arising from a doubly degenerate zone-boundary phonon mode. The resulting energy landscape exhibits four energetically equivalent wells, described by left- and right-handed chiral space groups. Additionally, we demonstrate that substituting K with larger cations (e.g., Na, Rb, Cs) and replacing Ni with Ag or Au hardens this soft mode, consistent with experimental observations. Our calculations further show that the resulting instability may be externally tuned with the help of hydrostatic pressure and epitaxial strain, and we quantify the effect of these external stimuli by calculating the energy difference between the chiral and achiral structures and the behavior of the O-K-O bonding angle. In particular, we show that the chirality should disappear above ~1 GPa or 3% tensile epitaxial strain. On the other hand, the chiral phases are additionally softened if compressive epitaxial strain is present. We discuss the effect of pressure and strain on other compounds undergoing an achiral-to-chiral transition, unveiling a possible general strategy to control chiral instabilities in materials.

DOI: 10.1103/PhysRevB.111.174102

I. INTRODUCTION

The absence of improper symmetry operations in periodic solids indicates that these systems are chiral, namely it is not possible to overlap a right-handed and a left-handed configuration via rotations and translations. Further, periodic solids are enantiomorphic if their structure is described by one of the 11 pairs of enantiomorphic space groups [1–3]. In this case, the handedness is determined by the space group. In recent years there has been a growing interest in investigating certain chiral effects (both in real space and spin space) in crystals such as the chiral induced spin selectivity (CISS) and spin spirals [4,5], polar [6] and magnetic skyrmions [7,8], topological states [9,10], and chiral phonons [11–13] to mention a few. Noticeably, the crystallization process fixes the chirality and associated properties in most of these instances.

Spontaneous symmetry breaking has been a rich source of significant discoveries in condensed matter physics, underpinning phenomena like ferroelectricity, magnetism, and superconductivity [14]. However, the exploration of the spontaneous emergence of chirality from an achiral solid phase within this framework is still limited. Nevertheless, a time-reversal even chiral irreducible representation (IRREP) or order parameter can be formally defined [15], so that a group-subgroup relationship of the type achiral → chiral between two phases is a physical possibility [16]. Despite the recent experimental reports about the spontaneous formation of chiral domains observed in certain materials [17–22] below a critical temperature, many questions remain to be answered about their physical origin, properties, and the way they can be controlled. In the context of structural orders and phonons in particular, the possibility of controlling the handedness of a chiral eigenmode via linearly polarized THz light has been proposed [23]. In particular, the chiral mode is coupled to a pair of infrared (IR) modes, which can be activated by an electric field. A recent experimental realization of this phenomenon has instead been realized in BPO_4 [24], where the chiral phonon mode, with the symmetry of the polarization along the c axis, has also been activated at second order in the IR phonon displacements via linearly polarized THz light. Controlling the handedness of a chiral phonon mode via electric fields is clearly facilitated when the reference undistorted phase belongs to the axial space groups, as it is the case of BPO_4 [24] and $Pb_5Ge_3O_{11}$ [22,25,26] (space groups $I\bar{4}$, $P\bar{6}$). While looking for axiality in the parent phase is a valid material search strategy in this context, we also need to point out that chiral crystals are in general neither polar nor axial. If a chiral order is not associated with a polar space group or with a finite spontaneous polarization, then it cannot be controlled by an electric field the same way as in the case of switchable ferroelectric materials [22,27]. Hence, it is important to understand how and in which system a purely chiral structural order can be triggered and its handedness manipulated.

In this study, we take the next step by investigating the achiral-to-chiral enantiomorphic phase transition observed in potassium oxonickelate, K_3NiO_2 (KNO) [28,29]. Using symmetry analysis and density functional theory (DFT) calculations, we show that a soft zone boundary phonon mode triggers the emergence of chirality in this material with four well-like shapes in the energy landscape. We also show that this soft phonon may persist upon chemical substitution of the potassium and/or nickel ion, although the amplitude and consequently the critical temperature of the transition strongly depend on the ionic mass, as also experimentally reported [29]. We then explore the relative energies of the chiral and achiral phases as a function of hydrostatic pressure, tensile strain, and compressive strain. This strategy of using pressure or strain to tune the energy landscape of the chiral instability is also discussed in the context of different materials. Importantly, KNO and similar compounds develop purely chiral phases, in the sense that no spontaneous polarization appears below the critical temperature, unlike other crystals such as, for instance, $Pb_5Ge_3O_{11}$ [21,22]. This, in addition, allows us to disentangle chiral and polar phenomena. Considering the degenerate nature of the instability, we propose a transition path for handedness interconversion, mediated for example by a circularly polarized electromagnetic field, which can also be influenced by pressure and strain.

II. METHOD

The calculations for the K_3NiO_2 (KNO) compound were carried out using the VASP (v5.4) code [30] and the PBE functional [31]. We have adopted a cutoff of 550 eV, a $6 \times 6 \times 6$ k-point grid, and a 10^{-6} eV tolerance over the self-consistent convergence. We have employed a Hubbard-U correction within the scheme devised by Dudarev *et al.* [32]. With the help of the method of Cococcioni *et al.* [33], we have obtained $U = 4.2$ eV. Finally, the symmetry and energy invariants analysis has been performed with the help of the ISODISTORT [34] software. The phonon spectrum has been calculated with the help of the Phonopy software [35,36] and of a $2 \times 2 \times 2$ supercell (96 ions), and the interpolation and plots were made using the postprocessing tools of the ABINIT suite [37].

The initial magnetic moments on the nickel sites are $+1\,\mu_B$, which are found stable upon relaxation. Calculations using different initial magnetic models show very little impact on the structural parameters, the electronic structure, and the energies. Hence, the numerical results discussed in the following have been carried out assuming a ferromagnetic order. This is consistent with our calculation of the superexchange interactions with the TB2J code [38] where the largest value is found to be only 0.02 meV, and with experiments where paramagnetism has been measured across the whole 1.8 K–400 K temperature range [29].

The calculations of the phonon band structure of other A_3BO_2 stoichiometries (A = Na, K, Rb, and Cs; B = Ag, and Au) in the high symmetry $P4_2/mnm$ structure were done using the ABINIT code [37,39], the norm-conserving pseudopotentials of the PseudoDojo server (PBEsol v0.4) [40,41], and with a plane wave cutoff energy of 50 Ha and a $6 \times 6 \times 6$ k-points grid.

III. SOFT PHONON MODES IN THE $P4_2/mnm$ REFERENCE PHASE

The alkali oxometallates A_3MO_2 are notable for their low coordination numbers of both the alkali A^+ cations and the transition metal M^+ cations, as well as the unusually low oxidation state of the transition metal. In many of these compounds, the M^+ cations (e.g., Fe^+, Co^+, Ni^+) are arranged into dumbbell-shaped MO_2^{3-} units [28,29,42], which resemble the BN_2^{3-} units found in Li_3BN_2 and are characterized by strong covalent bonding [43]. These almost linear MO_2^{3-} units are typically packed perpendicular to one another, with alkali A^+ cations in two to four coordinate interstitial sites [42,44–46]. The alkali oxonickelates typically adopt a high symmetry structure of $P4_2/mnm$ symmetry with two A^+ cation sites: $A(1)$ is in the center of distorted $A(1)O_4$ tetrahedra whilst $A(2)$ sites are effectively two-coordinate forming linear O – M – O – $A(2)$ – O – M – O chains (see Fig. 1)

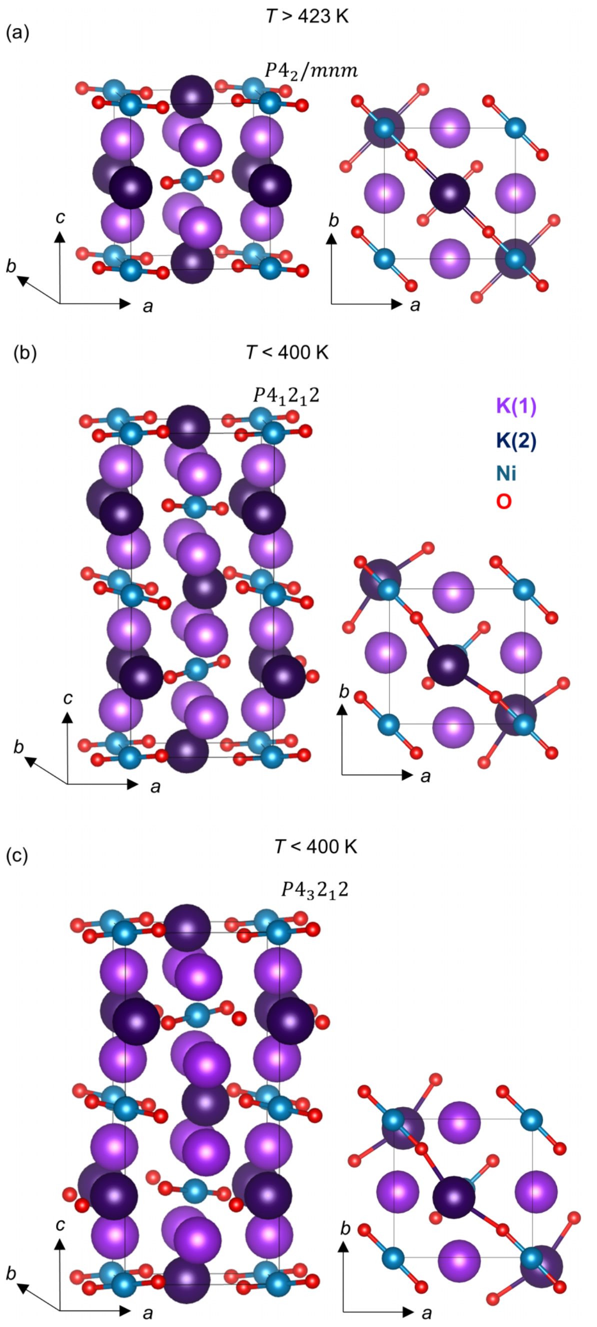

FIG. 1. Schematic showing (a) high temperature $T > 423$ K $P4_2/mnm$ achiral phase of K_3NiO_2; panels (b) and (c) show low temperature $T > 400$ K chiral phases of $P4_12_12$ and $P4_32_12$ symmetries with K(1), K(2), Ni, and O sites shown in light and dark purple, blue, and red, respectively. K(2) - O - Ni - O chains are highlighted.

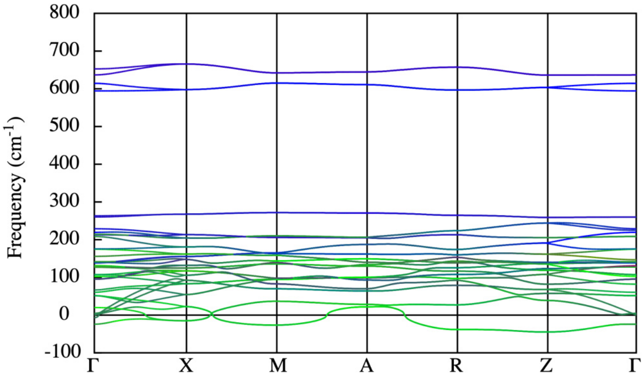

FIG. 2. Calculated phonon band structure of K_3NiO_2 in its high-symmetry P4$_2$/mnm phase. The high symmetry *k* points are Γ (0, 0, 0), X (1/2, 0, 0), M (1/2, 1/2, 0), A (1/2, 1/2, 1/2), R (1/2, 0, 1/2), and Z (0, 0, 1/2). The color of the different branches are weighted according to the contribution of each chemical species to the dynamical matrix eigenvector (red for the Ni atom, green for the K atom, and blue for the O atom).

[28,29]. Cs_3NiO_2 retains this achiral high symmetry structure down to at least room temperature, but Rb_3NiO_2 undergoes a phase transition to a chiral phase at 390 K [28].

Careful temperature-dependent structural characterization showed that K_3NiO_2 undergoes a first order phase transition (between 400–423 K) from the high temperature $P4_2/mnm$ phase to a low temperature enantiomorphic phase of either $P4_12_12$ or $P4_32_12$ symmetry. The phase transition is characterized by displacements of the K(2) ions (perpendicular to the linear chains described above) giving O – K(2) – O angles <180°. (Atomic displacement parameters refined from high temperature data suggest either static or dynamic disorder consistent with this distortion above the phase transition temperature) [29]. The covalently bonded NiO_2^{3-} units remain close to linear through this phase transition, but rotate very slightly about the [110]/[11-0] directions (Fig. 1). Also, the experimental c/a ratio goes from 1.18 to 2.28 from 500 K to 50 K.

Our symmetry adapted mode (SAM) analysis of the unoptimized experimentally reported structures (500 K and 50 K) [29] shows that the corresponding symmetry-lowering structural deformation decomposes into a main zone boundary mode with Z_4 irreducible representation (IRREP), and secondary modes with Γ_1^- (pseudoscalar) and Γ_1^+ (invariant) representations. The atomic displacements associated with the Z_4 IRREP are 0.57, 0.23, 0.22, and 0.05 Å/ion, for K(2), K(1), O, and Ni atoms, respectively (all displacements with the exception of the O one are in plane). Conversely, the pseudoscalar and invariant zone center symmetry modes can, respectively, be described by a 0.007 Å/ion displacement of the K(1) atom along the out-of-plane direction, and by an in-plane 0.007 Å/ion displacement of the O atoms. We can conclude that the Z_4 mode is both the origin and main descriptor of the phase transition in KNO.

To understand the physical origin of this Z_4 irrep appearing in the SAM analysis, we calculated the phonon band structure in the $P4_2/mnm$ phase, shown in Fig. 2. Unstable modes can be found at and in between Γ and all the zone boundaries except the A point. Among them, we identify a doubly degenerate unstable mode at the Z point with the imaginary frequency $\omega_Z = 45i\,\mathrm{cm}^{-1}$ and the Z_4 irreducible representation, hence, consistent with the previous SAM analysis of the experimental phases. To check which mode gives the lowest energy, we condensed and relaxed all the unstable modes from the zone boundary (Table I) and found that the Z_4 mode leads to the most stable low-symmetry configuration, in agreement with experiments [29].

TABLE I. Unstable phonon modes irrep and frequencies of the DFT relaxed high symmetry $P4_2/mnm$ phase of K_3NiO_2 at Γ and the zone boundary, and the associated $\Delta E = E(\mathrm{mode}) - E(P4_2/mnm)$ gain of energy when condensed and fully relaxed. The $P4_2/mnm$ cell is here adopted as a reference unit.

Mode irrep	freq.(cm^{-1})	ΔE (meV/f.u.)
Γ_5^-	27i	−3.0
X_2	15i	−3.7
$M_2^-M_3^-$	27i	−4.2
R_1^-	38i	−3.6
Z_4	45i	−8.9

In the case of the Z_4 instability, the dependence of ΔE on the *U* parameter is weak, as suggested by ΔE (U = 3.2 eV) = 7.7 meV/f.u. and ΔE (U = 5.2 eV) = 10.4 meV/f.u. upon full structural relaxation (formula unit refers to the $P4_2/mnm$ unit cell). We can notice that the Γ_1^- and Γ_1^+ present in the SAM analysis are not unstable modes of the high symmetry phase, which explains why they are secondary and much smaller in the SAM amplitudes. Hence, we can conclude that the chiral phase transition present in K_3NiO_2 is associated with the condensation of a soft phonon mode from the Z zone boundary point. Being focused on the chiral phase of our present interest, we will not study the other unstable modes throughout the rest of the paper, since none of them generate the experimental low temperature chiral structures.

We can characterize the low-symmetry structure that can be obtained by (i) projecting the soft Z mode and (ii) optimizing the structure. The DFT-obtained c/a ratio reads 1.15 in the reference phase and 2.3 in the chiral one. The effect of this Z_4 distortion in our geometry-optimized chiral model can be described in terms of (i) an in-plane helical displacement (0.4 Å/ion) of the K(2) atoms, which belong to the Ni-O-K(2)-O linear chains and localize at the 2*b* site in the $P4_2/mnm$ phase [29], as shown in Fig. 1; (ii) a smaller distortion of the tetrahedral K(1) atoms (0.17 Å/ion, from the 4*d* site in the $P4_2/mnm$ phase); (iii) an out-of-plane (0.14 Å/ion) oxygen displacement. As a consequence, below T_c the O - K - O chain bond angle becomes smaller than 180°, whilst the NiO_2^{3-} units remain close to linear, in agreement with experimental structure reports [29,47]. A secondary Γ_1^- SAM, observed upon optimization of the chiral structures, is instead solely constituted by a small displacement (0.006 Å/ion) of tetrahedrally coordinated K atoms along the *c* axis, consistent with the symmetry analysis of the experimental phases. Finally, an invariant Γ_1^+ mode is represented by a negligible oxygen displacement along the direction of the Ni-O-K(2)-O chains (−0.001 and 0.001 Å/ion along the *x* and *y* axes,

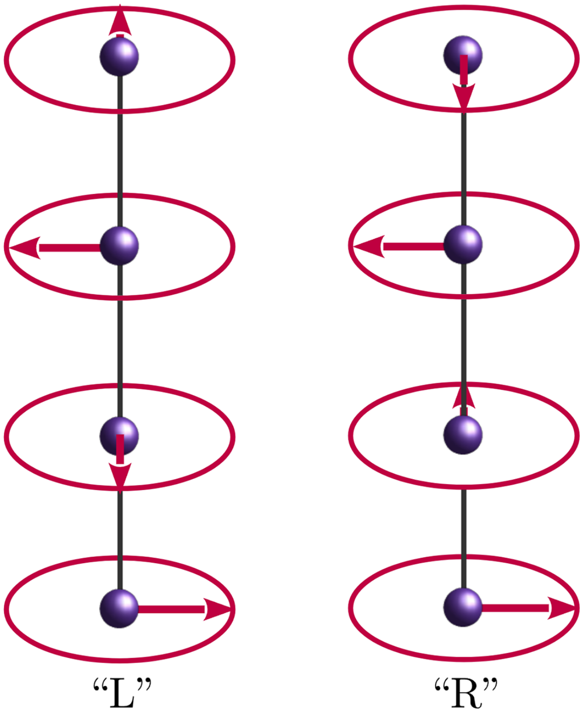

FIG. 3. Scheme of the helical atomic distortions (red arrows, the circles are guide to the eye) characterizing the displacive phase transition of K_3NiO_2 from the $P4_2/mnm$ reference phase to the low symmetry $P4_32_12$ and $P4_12_12$ enantiomorphic structures.

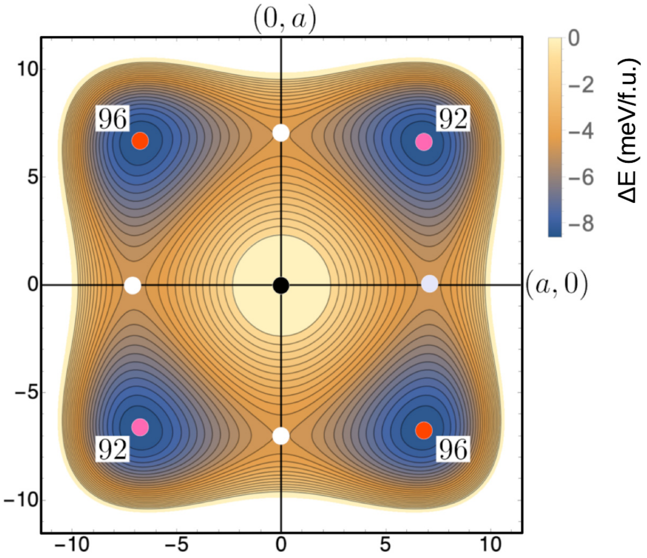

FIG. 4. Schematic 2D projection of the surface energy given by condensing the two-dimensional Z_4 mode (amplitudes in arbitrary units). The central black circle corresponds to the high symmetry $P4_2/mnm$ phase. The *Cmcm* (no. 63) energy minimum points are highlighted with white circles. Red and pink filled circles indicate the degenerate ground state points in the $P4_32_12$ (no. 96) and $P4_12_12$ (no. 92) enantiomorphic phases, respectively. The energy landscape has been fitted on the invariant $U = \alpha(a^2 + b^2) + \beta(a^2 + b^2)^2 + \gamma(a^4 + b^4)$ polynomial for the general domain direction and amplitude (a, b) and with α, β, and γ the fitted coefficients.

respectively). The description of the calculated primary and secondary order parameters therefore agrees reasonably well with the experimental results [28,29,47]. Hence, the main atomic distortions of the Z_4 mode in one of its chiral domain can be seen as in-plane atomic motions that rotate by 90 degrees from atomic plane to atomic plane along the z direction, as illustrated in Fig. 3. Those atomic motions form a spiral that preserves the fourfold screw rotation of the parent phase, hence giving the left- and right-handed enantiomorphic structures (Fig. 3).

Since the Z_4 soft boundary mode is doubly degenerate we have the following possible domains depending on the condensation of the mode along the (x, y) directions: (±a, 0), (0, ±a), (±a, a), (±a, −a), and (a, b) with a ≠ b. The (±a,0) and (0,±a) cases are not chiral and they possess *Cmcm* symmetry. The (a, a) and (−a, −a) distortions give the $P4_12_12$ phase, and the (−a, a) and (a, −a) cases induce the $P4_32_12$ phase. Noticeably, the latter enantiomorphic space groups correspond to the experimentally observed low symmetry phase. Finally, the generic (a, b) case gives a chiral nonenantiomorphic phase with $C222_1$ space group symmetry (i.e., the left and right handed structures share the same symmetry operations), which retains only the twofold rotations.

Because of this degeneracy, we can build arbitrary linear combinations of eigenvectors and calculate the energy as a function of their amplitude, as illustrated in Fig. 4. We can see that four degenerate minima of the energy can be found and are associated with the enantiomorphic chiral space group domains (a, a), (−a, −a), (a, −a), and (−a, a). The *Cmcm* cases instead form four local saddle points in between the left- and right-handed symmetries. Upon relaxation and considering a 1 × 1 × 2 supercell commensurate to the Z mode, the energy gain associated with the chiral phases is 17.9 meV, while the gain related to the *Cmcm* structures gives 12.2 meV. This confirms the experimental result that the enantiomorphic phases are the low-symmetry ground states. Given that these values are rather close, it is possible that a competition between chiral tetragonal and achiral orthorhombic phases may be present Finally, the closeness between the handed and orthorhombic energies suggests that a $P4_12_12 \leftrightarrow Cmcm \leftrightarrow P4_32_12$ transition path for handedness interconversion may be possible under a stimulus (namely a chiral electromagnetic field) that splits the right- and left-handed energies. The theoretical exploration of this possibility has been discussed in a separate work [48].

IV. ELECTRONIC PROPERTIES

The electronic density of states (DOS) near the Fermi level of the $P4_2/mnm$ phase of KNO is shown in Fig. 5. It is mainly populated by hybridized O-2p/Ni-3d valence and K-3d conduction states within the ground state low-spin configuration. The selected $U = 4.2$ eV opens a 1.66 eV band gap between $\{d_{xz}, d_{yz}\}$ valence and d_{z^2} conduction levels. We find the density of states to be negligibly affected by the phase transition, and in particular that a negligible $p-d$ transfer of charge takes place. This is in agreement with the rather nominal computed Born effective charges reported in Table II, which mimic the oxidation states of Ni, K, and O (+1, +1, and −2). This suggests a short-range interaction mechanism

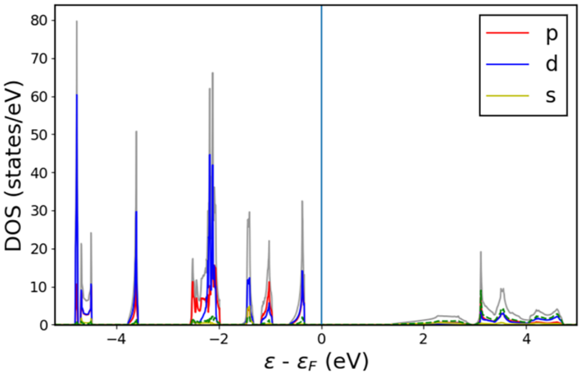

FIG. 5. Partial electronic density of states near the Fermi level ($P4_2/mnm$ phase). The dashed green curve represents K states and the gray curve the total DOS.

for the emergence of chirality, in agreement with the zone boundary nature of the soft phonon mode [49].

V. EFFECT OF CHEMICAL PRESSURE

We have computed the phonon band structure of A_3BO_2 stoichiometry (A = Na, K, Rb, and Cs; B = Ag and Au) in the high symmetry $P4_2/mnm$ structure of K_3NiO_2 to probe the effect of chemical pressure on the unstable phonon modes [50]. We report our results in Fig. 1 in the Supplemental Material [51], where we can see that the chiral Z_4 phonon mode is always unstable. Nevertheless, we can observe that the amplitude of the unstable chiral phonon mode decreases with the size of the A cation. In particular, the high symmetry achiral structure is nearly stable in the A = Cs case. A similar effect is observed for all the other soft modes, which disappear for A cations heavier than Rb. The same is observed upon increasing the size of the B cation from Ag to Au, i.e., the instabilities are reduced with increasing cation size. Hence, the Z_4 chiral instability is a common feature of the $P4_2/mnm$ structure and increasing the size of the cell through the size of the cations tends to stabilize the high symmetry $P4_2/mnm$ structure.

TABLE II. Calculated Born effective charges of nonequivalent Ni, K, and O ions in the $P4_2$/mnm high symmetry phase.

Atom	site sym.	
Ni_1	2a	$\begin{pmatrix} 0.25 & 1.66 & 0.00 \\ 1.66 & 0.25 & 0.00 \\ 0.00 & 0.00 & -1.10 \end{pmatrix}$
K_1	4d	$\begin{pmatrix} 1.06 & -0.04 & 0.00 \\ 0.04 & 1.06 & 0.00 \\ 0.00 & 0.00 & 1.10 \end{pmatrix}$
K_2	2b	$\begin{pmatrix} 1.34 & -0.22 & 0.00 \\ -0.22 & 1.34 & 0.00 \\ 0.00 & 0.00 & 1.19 \end{pmatrix}$
O_1	4f	$\begin{pmatrix} -1.86 & -0.84 & 0.00 \\ -0.84 & -1.86 & 0.00 \\ 0.00 & 0.00 & -1.15 \end{pmatrix}$

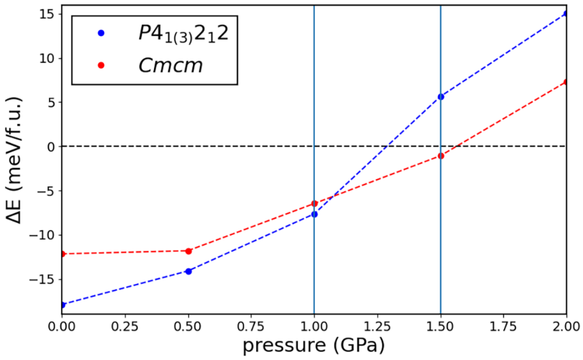

FIG. 6. Energy differences $\Delta E = E(P4_2/mnm)$-E(X)($X = P4_{1,3}2_12$, $Cmcm$) as a function of an applied hydrostatic pressure. A possible phase transition from chiral to a $Cmcm$ phase may occur at ~1 GPa.

VI. HYDROSTATIC PRESSURE AND EPITAXIAL STRAIN

Considering the geometric nature of the chiral order parameter, mechanical and elastic effects can be expected to strongly affect the energy surface associated with the Z_4 instability. In particular, epitaxy and pressure can influence the behavior of the Ni-O-K-O bond angle that correlates with the soft phonon-induced chiral distortion.

By looking first at the effect of hydrostatic pressure (see Fig. 6), we see that even a tiny amount of hydrostatic pressure (above a value between 1.0 and 1.5 GPa) hardens the chiral mode and destroys the phase transition. Below 1.0 GPa, the (a, a) and (a, −a) domains are the most stable, while a possible pressure-induced transition to an orthorhombic $Cmcm$ phase may take place at ~1.0 GPa. This achiral phase corresponding to the (a, 0) and (0, a) domains may be stable in the 1.0–1.5 GPa interval, above which all phases related to the Z mode are less stable compared to the $P4_2/mnm$ reference. This hardening under pressure may correlate well with the observed decrease of the transition temperature upon replacing K^+ with larger Rb^+ or Cs^+ ions as discussed above, namely in Rb_3NiO_2 (T_c = 390 K) and Cs_3NiO_2 (achiral at room temperature) [29] and from our chemical pressure result reported in Sec. V.

Conversely, an even more nuanced effect can be observed in the presence of strain (Fig. 7). Indeed, the Z_4 mode is hardened if the applied in-plane $\epsilon_{xx} = \epsilon_{yy}$ lattice deformation is tensile, while it is softened if it is compressive, as shown in Fig. 7. These results stem from a tension-compression asymmetry of the energy response in both the high and low symmetry phases. Nevertheless, the energy of the $P4_2/mnm$ high symmetry phase is always larger than the $P4_{1(3)}2_12$ chiral phase in the range of distortions considered here. Noticeably we find that the polar Γ_5^- instability reported in Table I persists under both compressive and tensile $\epsilon_{xx} = \epsilon_{yy}$ strain, with $\Delta E(P4_2/mnm \rightarrow \Gamma_5^-) = -3.8$ eV upon 3% compression and −2.3 meV upon 3% tension. Moreover, and since the irreducible decomposition of the strain tensor does not include the Γ_5^- IRREP, the direction of this polar mode ought to be preserved under a distortion of the lattice. While both values lie higher than the corresponding chiral state energy, it is

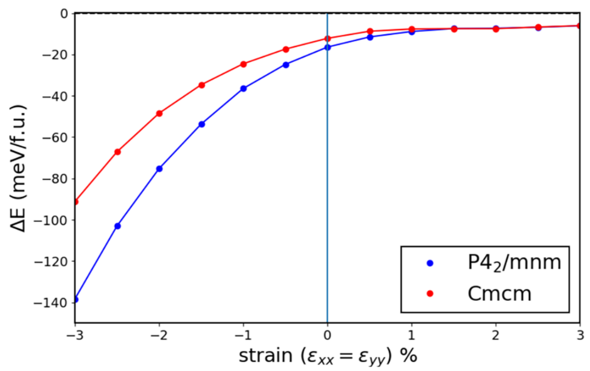

FIG. 7. $P4_{1,3}2_12$ and *Cmcm* energies relative to the high symmetry phase as a function of epitaxial in-plane strain. The in-plane lattice parameters are constrained, while the out-of-plane lattice parameter and the ion coordinates are relaxed.

possible that ferroelectricity may coexist with chirality under tension (at 3% or larger values).

To further characterize the role of pressure and strain on the chirality of K_3NiO_2, we evaluate the Ni-O-K-O planar angle which geometrically characterizes the Z_4 soft phonon mode. The corresponding plots are reported in the Supplemental Material [51]. In particular, we find that the O-K-O angle bends following a $\sim\sqrt{P}$ law with respect to the hydrostatic pressure P. On the other hand, the same angle increases or decreases linearly with respect to 180° (high symmetry phase) if compressive or tensile strain is present. Therefore, it appears that the relevant energy scales for the emergence and control of chiral features in K_3NiO_2 and analogous A_3BO_2 compounds sharing the same symmetries [51] may be efficiently controlled via epitaxial growth, provided that a suitable substrate is selected.

VII. POSSIBLE ENANTIOSELECTIVITY IN KNO-LIKE SYSTEMS

While pressure and epitaxy are likely to affect the critical temperature and possibly the kinetics and domain behavior, they may also have an indirect effect over the selection of a preferred handedness, which we theorize may be achieved below T_c in this and analogous systems (where the chiral order stems from a degenerate instability) [48]. Following Ref. [48], a chiral electromagnetic (EM) field may be used to select either a right- or a left-handed phase, with the possibility of converting one into the other through an intermediate *Cmcm* [(a, 0) or (0, a)] transition state associated with the degeneracy of the Z_4 representation. While the instability does not couple directly to an EM field, it can interact with symmetry modes belonging to the polar **P** and axial (parity even) **G** irreducible representations of the $4/mmm$ parent point group. Among the allowed coupling terms, the

$$V_{\text{flip}} = ab[\lambda_{xy}(P_xG_x + P_yG_y) + \lambda_z P_z G_z] \tag{1}$$

free energy invariant is a source of enantioselectivity, since it can harden or soften the (a, a) and (a, −a) domains in an asymmetric fashion [48]. It is to be stressed that unlike compounds possessing intrinsic axiality, a linearly polarized field may not favor one enantiomorph over the other, in particular if the right hand side of Eq. (1) vanishes. For instance, if a static electric field is used, the generated electric toroidal moment reads $\mathbf{G}_{xy} \propto \mathbf{P}_{xy} \times \mathbf{P}_z$, so that $P_xG_x + P_yG_y = 0$. An alternative symmetry-allowed solution involving linearly polarized fields could be that of exploiting the coupling between a static polarization and a high-frequency infrared mode $\mathbf{u}$. Indeed, the ensuing toroidal vector $\mathbf{G}_z \propto \mathbf{P}_{x(y)} \times \mathbf{u}_{y(x)}$ leads in principle to a nonvanishing P_zG_z. Otherwise, a circularly polarized (CP) electromagnetic field seems to be required, and its effect on the Z_4 energy landscape understood as follows. We can consider a CP pulse $\mathbf{E}(z, t)$ with components along the x and y directions such as

$$\begin{aligned} \mathbf{E}(z, t) &= \mathbf{E}_0 e^{-t/\tau} e^{-\kappa z}[\sin(u_z)\hat{\mathbf{x}} \pm \cos(u_z)\hat{\mathbf{y}}], t \geqslant 0 \\ \mathbf{E}(z, t) &= 0, t < 0, \end{aligned} \tag{2}$$

where $u_z \equiv k_z \cdot z - \omega \cdot t$. Therefore, Eq. (1) becomes

$$V_{\text{flip}}(z, t) = \pm\lambda_{xy} ab[e^{-2t/\tau} e^{-2\kappa z} \chi_e \chi_g \cdot |\mathbf{E}_0|^2 k_z]\Theta(t), \tag{3}$$

where $\Theta(t)$ is the Heavyside step function and χ_e, χ_g are the electric and toroidal susceptibilities [48]. Depending on the handedness of the CP field, V_{flip} may thus asymmetrically favor either the $P4_12_12$ or the $P4_32_12$ phase [48]. Importantly, this enantioselective mechanism may occur below the crystallization temperature and possibly below the phase transition temperature as well, taking the features of a hysteresis process. This handedness conversion phenomenon, which could be detectable if measurements of gyrotropic quantities such as the natural optical activity are performed, is clearly influenced by the $P4_{1,3}2_12$-*Cmcm* energy difference. Indeed, the reduction of this energy difference – as may be obtained under tension or hydrostatic compression approaching 1 GPa - likely suggests a decrease of the electromagnetic coercive field required to flip the handedness of the system below the critical temperature.

VIII. CHIRAL TRANSITIONS IN OTHER COMPOUNDS

Controlling the energies of the various chiral and orthorhombic phases via pressure and strain has effects on relevant physical parameters such as gyrotropic properties and the temperature of the phase transition T_c. Moreover, it is reasonable to hypothesize that mechanical stimuli affecting bond angles and lengths are well suited in general to control the features related to spontaneous structural chiral orders.

For instance, TeO_2 crystallizes under either the $P4_12_12$ or the $P4_32_12$ chiral space groups [52–54] (α phase), although orthorhombic β and γ polymorphs with *Pbca* and $P2_12_12_1$ symmetries have also been detected and studied [55]. It has also been shown [56] that a chiral → orthorhombic transition can be mediated by pressure near 1 GPa. Interestingly, a rutile $P4_2/mnm$ high symmetry parent structure has recently been found under epitaxial growth on a FeTe substrate [54]. Similar to K_3NiO_2, this TeO_2 rutile phase has recently been shown to have a zone boundary unstable phonon mode that can drive a displacive $P4_2/mnm$ to $P4_12_12$ or $P4_32_12$ transition [57].

Another example is SiO_2 cristobalite, for which the high-temperature β structure is cubic ($Fd\bar{3}$m), but a chiral metastable low-symmetry α configuration, characterized by helices with either $P4_12_12$ or $P4_32_12$ symmetries [58–61] is found below 530 K [62]. A soft zone boundary $X = (0,1,0)$ phonon mode drives this phase change; nevertheless, a sizable (∼3–4%) volume decrease is observed below the critical temperature [60], suggesting a non-negligible influence of pressure on this system as well. It is indeed to be noticed that among the SiO_2 polymorphs, cristobalite is the one with the largest compressibility [63].

Finally, known compounds where a chiral order can be induced at a finite T_c are spinels. Most studies on spinels, with general formula AB_2O_4 (A^{2+}, B^{3+} cations), are limited to "normal" (with A^{2+} and B^{3+} ions on tetrahedral and octahedral sites, respectively) or "inverse" spinels (A^{2+} ions on octahedral sites, B^{3+} ions on both sites), with cubic structures described by $Fd\bar{3}m$ symmetry. However, by clever choice of chemistry, chiral spinels may be designed, and achiral-chiral phase transitions may be observed, depending on the origin of the chirality. Chiral spinels can be synthesized by relying on ordering of the B site cations [64] (e.g., for $LiZnNbO_4$ [65] or $Li_2NiGe_3O_8$ [66,67]), and can also result from electronically driven structural distortions (e.g., in $MgTi_2O_4$) [68,69]. In addition, an important effect of the substrate on the kinetics of the cubic → chiral phase transition in Mg_2XO_4 (X= Ti, Ge) thin films has been detected [70], where an epitaxial strain is generated at finite temperature due to the thermal expansion coefficients mismatch between spinel and substrate. Interestingly, the emergence of electron diffraction features consistent with the onset of chirality in Mg_2GeO_4 is epitaxy-driven, since the bulk cubic structure is assumed to be stable [70].

IX. CONCLUSIONS

Through *ab initio* calculations, we have demonstrated that a degenerate soft zone-boundary phonon mode can drive a transition in crystals to a purely chiral phase. Using the K_3NiO_2 compound as a model system, we have shown that its initial $P4_2/mnm$ symmetry is lowered to the enantiomorphic symmetries $P4_12_12$ and $P4_32_12$ through the activation of a soft mode with Z_4 irreducible representation. Furthermore, we have found that the chiral ground state phases are close in energy to competing orthorhombic $Cmcm$ phases. K_3NiO_2 belongs to a class of A_3BO_2 materials, and we have calculated the phonon band structure in the $A =$ Na, K, Cs, Rb and $B =$ Ag, Au cases. In agreement with experiments, our calculations suggest that the critical temperature T_c decreases with the size of the A cation, hence chemical substitution could be a powerful tool to explore chiral orders in these systems.

Additionally, we have shown that the energy landscape and, hence, the phase diagram, can be controlled by epitaxial strain and hydrostatic pressure. Indeed, while pressure and tensile strain can be used to harden the chiral mode and destroy the chiral order in favor of competing achiral ($P4_2/mnm$ or orthorhombic) phases, compressive strain further softens and stabilizes the chirality. A strong sensitivity of chiral symmetries with respect to mechanical stimuli that affect bond lengths and angles has also been measured in other compounds, for instance SiO_2 cristobalite [60,63] and some spinel oxides [70]. Overall, this also suggests that pressure and epitaxy are valid tools to control or trigger chiral effects in materials. Finally, we propose K_3NiO_2 and analogous A_3BO_2 systems with the same structure as suitable platforms to explore the concepts of (i) chirality as an order parameter, and (ii) that of enantioselectivity in chiral materials [3,48] lacking intrinsic axial and polar orders and beyond the ultrafast regime.

ACKNOWLEDGMENTS

Computational resources have been provided by the Consortium des Équipements de Calcul Intensif (CÉCI), funded by the Fonds de la Recherche Scientifique (F.R.S.-FNRS) under Grant No. 2.5020.11. M.F. and E.B. acknowledge FNRS for support and the PDR project CHRYSALID No. 40003544. We also thank the Pittsburgh Supercomputer Center (Bridges2) and San Diego Supercomputer Center (Expanse) through allocation DMR140031 from the Advanced Cyberinfrastructure Coordination Ecosystem: Services & Support (ACCESS) program, which is supported by National Science Foundation Grants No. 2138259, No. 2138286, No. 2138307, No. 2137603, and No. 2138296. We acknowledge the computational resources provided by WVU Research Computing's Dolly Sods HPC cluster, partially supported by NSF Grant No. OAC-2117575. Additionally, we are grateful for funding from the West Virginia Higher Education Policy Commission under the Research Challenge Grant Program 2022 (Award RCG No. 23-007) and the NASA EPSCoR Program (Award No. 80NSSC22M0173).

[1] M. Nespolo, M. I. Aroyo, and B. Souvignier, Crystallographic shelves: Space-group hierarchy explained, J. Appl. Crystallogr. **51**, 1481 (2018).

[2] H. Flack, Chiral and achiral crystal structures, Helv. Chim. Acta **86**, 905 (2003).

[3] E. Bousquet, M. Fava, Z. Romestan, F. Gómez-Ortiz, E. E. McCabe, and A. H. Romero, Structural chirality and related properties in periodic inorganic solids: Review and perspectives, J. Phys.: Condens. Matter **37**, 163004 (2025).

[4] S.-H. Yang, R. Naaman, Y. Paltiel, and S. S. P. Parkin, Chiral spintronics, Nat. Rev. Phys. **3**, 328 (2021).

[5] F. Evers, A. Aharony, N. Bar-Gill, O. Entin-Wohlman, P. Hedegård, O. Hod, P. Jelinek, G. Kamieniarz, M. Lemeshko, K. Michaeli, V. Mujica, R. Naaman, Y. Paltiel, S. Refaely-Abramson, O. Tal, J. Thijssen, M. Thoss, J. M. van Ruitenbeek, L. Venkataraman, D. H. Waldeck *et al.*, Theory of chirality induced spin selectivity: Progress and challenges, Adv. Mater. **34**, 2106629 (2022).

[6] J. Junquera, Y. Nahas, S. Prokhorenko, L. Bellaiche, J. Íñiguez, D. G. Schlom, L.-Q. Chen, S. Salahuddin, D. A. Muller, L. W. Martin, and R. Ramesh, Topological phases in polar oxide nanostructures, Rev. Mod. Phys. **95**, 025001 (2023).

[7] A. N. Bogdanov and U. K. Rößler, Chiral symmetry breaking in magnetic thin films and multilayers, Phys. Rev. Lett. **87**, 037203 (2001).

[8] A. Fert, N. Reyren, and V. Cros, Magnetic skyrmions: Advances in physics and potential applications, Nat. Rev. Mater. **2**, 17031 (2017).

[9] G. Chang, B. J. Wieder, F. Schindler, D. S. Sanchez, I. Belopolski, S.-M. Huang, B. Singh, D. Wu, T.-R. Chang, T. Neupert, S.-Y. Xu, H. Lin, and M. Z. Hasan, Topological quantum properties of chiral crystals, Nat. Mater. **17**, 978 (2018).

[10] N. B. M. Schröter, S. Stolz, K. Manna, F. de Juan, M. G. Vergniory, J. A. Krieger, D. Pei, T. Schmitt, P. Dudin, T. K. Kim, C. Cacho, B. Bradlyn, H. Borrmann, M. Schmidt, R. Widmer, V. N. Strocov, and C. Felser, Observation and control of maximal Chern numbers in a chiral topological semimetal, Science **369**, 179 (2020).

[11] L. Zhang and Q. Niu, Chiral phonons at high-symmetry points in monolayer hexagonal lattices, Phys. Rev. Lett. **115**, 115502 (2015).

[12] K. Ishito, H. Mao, Y. Kousaka, Y. Togawa, S. Iwasaki, T. Zhang, S. Murakami, J.-i. Kishine, and T. Satoh, Truly chiral phonons in α-HgS, Nat. Phys. **19**, 35 (2023).

[13] H. Ueda, M. García-Fernández, S. Agrestini, C. P. Romao, J. van den Brink, N. A. Spaldin, K.-J. Zhou, and U. Staub, Chiral phonons in quartz probed by x-rays, Nature (London) **618**, 946 (2023).

[14] A. Beekman, L. Rademaker, and J. van Wezel, An introduction to spontaneous symmetry breaking, SciPost Phys. Lect. Notes 11 (2019).

[15] J. Hlinka, Eight types of symmetrically distinct vectorlike physical quantities, Phys. Rev. Lett. **113**, 165502 (2014).

[16] K. C. Erb and J. Hlinka, Symmetry guide to chiroaxial transitions, Phase Transitions **91**, 953 (2018).

[17] K. Kimura, M. Sera, and T. Kimura, A^{2+} cation control of chiral domain formation in $A(TiO)Cu_4(PO_4)_4$ (A = Ba, Sr), Inorg. Chem. **55**, 1002 (2016).

[18] P. Huang, Z. Xia, X. Gao, J. M. Rondinelli, X. Zhang, H. Zhang, K. R. Poeppelmeier, and A. Zunger, Ferri-chiral compounds with potentially switchable Dresselhaus spin splitting, Phys. Rev. B **102**, 235127 (2020).

[19] T. Hayashida, K. Kimura, D. Urushihara, T. Asaka, and T. Kimura, Observation of ferrochiral transition induced by an antiferroaxial ordering of antipolar structural units in $Ba(TiO)Cu_4(PO_4)_4$, J. Am. Chem. Soc. **143**, 3638 (2021).

[20] T. Hayashida, K. Kimura, and T. Kimura, Switching crystallographic chirality in $Ba(TiO)Cu_4(PO_4)_4$ by laser irradiation, J. Phys. Chem. Lett. **13**, 3857 (2022).

[21] M. Fava, W. Lafargue-Dit-Hauret, A. H. Romero, and E. Bousquet, Large and tunable spin-orbit effect of 6p orbitals through structural cavities in crystals, Phys. Rev. B **108**, L201112 (2023).

[22] M. Fava, W. Lafargue-Dit-Hauret, A. H. Romero, and E. Bousquet, Ferroelectricity and chirality in the $Pb_5Ge_3O_{11}$ crystal, Phys. Rev. B **109**, 024113 (2024).

[23] C. P. Romao and D. M. Juraschek, Phonon-induced geometric chirality, ACS Nano **18**, 29550 (2024).

[24] Z. Zeng, M. Först, M. Fechner, M. Buzzi, E. B. Amuah, C. Putzke, P. J. W. Moll, D. Prabhakaran, P. G. Radaelli, and A. Cavalleri, Photo-induced chirality in a nonchiral crystal, Science **387**, 431 (2025).

[25] H. Iwasaki, K. Sugii, T. Yamada, and N. Niizeki, $5PbO \cdot 3GeO_2$ crystal; A new ferroelectric, Appl. Phys. Lett. **18**, 444 (1971).

[26] H. Iwasaki, S. Miyazawa, H. Koizumi, K. Sugii, and N. Niizeki, Ferroelectric and optical properties of $Pb_5Ge_3O_{11}$ and its isomorphous compound $Pb_5Ge_2SiO_{11}$, J. Appl. Phys. **43**, 4907 (1972).

[27] V. Wadhawan, *Introduction to Ferroic Materials* (CRC Press, London, 2000).

[28] K. Ðuriš, U. Müller, and M. Jansen, K_3NiO_2 revisited, phase transition and crystal structure refinement, Z. Anorg. Allg. Chem. **638**, 737 (2012).

[29] K. Ðuriš, O. V. Magdysyuk, and M. Jansen, Syntheses, structures and magnetic properties of the alkali oxonickelates(i) A_3NiO_2 (A = K, Rb, Cs), Solid State Sci. **14**, 1399 (2012).

[30] G. Kresse and D. Joubert, From ultrasoft pseudopotentials to the projector augmented-wave method, Phys. Rev. B **59**, 1758 (1999).

[31] J. P. Perdew, K. Burke, and M. Ernzerhof, Generalized gradient approximation made simple, Phys. Rev. Lett. **77**, 3865 (1996).

[32] S. L. Dudarev, G. A. Botton, S. Y. Savrasov, C. J. Humphreys, and A. P. Sutton, Electron-energy-loss spectra and the structural stability of nickel oxide: An LSDA+U study, Phys. Rev. B **57**, 1505 (1998).

[33] M. Cococcioni and S. de Gironcoli, Linear response approach to the calculation of the effective interaction parameters in the LDA + U method, Phys. Rev. B **71**, 035105 (2005).

[34] H. T. Stokes, D. M. Hatch, B. J. Campbell, and D. E. Tanner, Isodisplace: A web-based tool for exploring structural distortions, J. Appl. Crystallogr. **39**, 607 (2006).

[35] A. Togo and I. Tanaka, First principles phonon calculations in materials science, Scr. Mater. **108**, 1 (2015).

[36] A. Togo, F. Oba, and I. Tanaka, First-principles calculations of the ferroelastic transition between rutile-type and $CaCl_2$-type SiO_2 at high pressures, Phys. Rev. B **78**, 134106 (2008).

[37] X. Gonze, B. Amadon, G. Antonius, F. Arnardi, L. Baguet, J.-M. Beuken, J. Bieder, F. Bottin, J. Bouchet, E. Bousquet, N. Brouwer, F. Bruneval, G. Brunin, T. Cavignac, J.-B. Charraud, W. Chen, M. Côté, S. Cottenier, J. Denier, G. Geneste *et al.*, The ABINITproject: Impact, environment and recent developments, Comput. Phys. Commun. **248**, 107042 (2020).

[38] X. He, N. Helbig, M. J. Verstraete, and E. Bousquet, TB2J: A python package for computing magnetic interaction parameters, Comput. Phys. Commun. **264**, 107938 (2021).

[39] A. H. Romero, D. C. Allan, B. Amadon, G. Antonius, T. Applencourt, L. Baguet, J. Bieder, F. Bottin, J. Bouchet, E. Bousquet *et al.*, ABINIT: Overview and focus on selected capabilities, J. Chem. Phys. **152**, 124102 (2020).

[40] D. Hamann, Optimized norm-conserving Vanderbilt pseudopotentials, Phys. Rev. B **88**, 085117 (2013).

[41] M. J. Van Setten, M. Giantomassi, E. Bousquet, M. J. Verstraete, D. R. Hamann, X. Gonze, and G.-M. Rignanese, The PSEUDODOJO: Training and grading a 85 element optimized norm-conserving pseudopotential table, Comput. Phys. Commun. **226**, 39 (2018).

[42] F. Bernhardt and R. Hoppe, Das erste oxoferrat(I): Zur konstitution von $K_3[FeO_2]$ und $K_3[NiO_2]$, Z. Anorg. Allg. Chem. **619**, 969 (1993).

[43] H. Yamane, S. Kikkawa, and M. Koizumi, High- and low-temperature phases of lithium boron nitride, Li_3BN_2: Preparation, phase relation, crystal structure, and ionic conductivity, J. Solid State Chem. **71**, 1 (1987).

[44] G. Wagner and R. Hoppe, Oxydation intermetallischer phasen: $Na_3[AuO_2]$ aus NaAu und Na_2O_2, Z. Anorg. Allg. Chem. **549**, 26 (1987).

[45] W. Losert and R. Hoppe, Ein neues oxocuprat (I): $K_3[CuO_2]$, Z. Anorg. Allg. Chem. **521**, 69 (1985).

[46] M. Sofin and M. Jansen, Rb_3CoO_2, a novel oxocobaltate(I) synthesized via the azide/nitrate route, Z. Anorg. Allg. Chem. **627**, 2115 (2001).

[47] A. Moeller, M. A. Hitchman, E. Krausz, and R. Hoppe, Synthesis, crystal structure and physical properties of KNa2[NiO2] and K3[NiO2] containing "linear" [NiO2]3- anions, Inorg. Chem. **34**, 2684 (1995).

[48] M. Fava, A. H. Romero, and E. Bousquet, Handedness selection and hysteresis of chiral orders in crystals, arXiv:2503.06782.

[49] G. A. Samara, T. Sakudo, and K. Yoshimitsu, Important generalization concerning the role of competing forces in displacive phase transitions, Phys. Rev. Lett. **35**, 1767 (1975).

[50] Although several of these compositions may crystallize with different asymmetric unit cells [71–74], we use the K_3NiO_2 structure to identify trends of the instabilities with respect to the cation masses. $U = 0$ is used in these systems.

[51] See Supplemental Material at http://link.aps.org/supplemental/10.1103/PhysRevB.111.174102 for additional plots related to the phonon band structure and to the structural behaviour under applied hydrostatic pressure and strain.

[52] J. Leciejewicz, The crystal structure of tellurium dioxide. a redetermination by neutron diffraction, Z. Kristallogr. - Cryst. Mater. **116**, 345 (1961).

[53] P. A. Thomas, The crystal structure and absolute optical chirality of paratellurite, α-TeO_2, J. Phys. C **21**, 4611 (1988).

[54] K. Peng, W. Ren, Y. Wu, H. Ru, S. Lu, A. Chen, P. Wang, X. Fang, H. Li, L. Chi, S. Ding, L. Wang, Y. Wang, and F. Li, Observation of metallic TeO_2 thin film with rutile structure on FeTe surface, J. Mater. Sci. **57**, 10225 (2022).

[55] M. Ceriotti, F. Pietrucci, and M. Bernasconi, *Ab initio* study of the vibrational properties of crystalline TeO_2: The α, β, and γ phases, Phys. Rev. B **73**, 104304 (2006).

[56] A. Jayaraman and G. A. Kourouklis, A high pressure Raman study of TeO_2 to 30 GPa and pressure-induced phase changes, Pramana **36**, 133 (1991).

[57] F. Gómez-Ortiz, A. H. Romero, and E. Bousquet, Pathways to crystal chirality an algorithm to identify new displacive chiral phase transitions, arXiv:2503.13076.

[58] N. R. Keskar and J. R. Chelikowsky, Structural properties of nine silica polymorphs, Phys. Rev. B **46**, 1 (1992).

[59] V. Dmitriev, V. Torgashev, P. Tolédano, and E. K. H. Salje, Theory of SiO_2 polymorphs, Europhys. Lett. **37**, 553 (1997).

[60] A. J. Leadbetter and A. F. Wright, The $\alpha - \beta$ transition in the cristobalite phases of SiO_2 and $AlPO_4$ I. X-ray studies, Philos. Mag. **33**, 105 (1976).

[61] D. M. Hatch and S. Ghose, The α-β phase transition in cristobalite, SiO_2, Phys. Chem. Miner. **17**, 554 (1991).

[62] M. T. Dove, Theory of displacive phase transitions in minerals, Am. Mineral. **82**, 213 (1997).

[63] R. T. Downs and D. C. Palmer, The pressure behavior of α cristobalite, Am. Mineral. **79**, 9 (1994).

[64] V. M. Talanov and V. B. Shirokov, Atomic order in the spinel structure – a group-theoretical analysis, Acta Crystallogr. Sect. A **70**, 49 (2014).

[65] S. J. Marin, M. O'Keeffe, and D. E. Partin, Structures and crystal chemistry of ordered spinels: $LiFe_5O_8$, $LiZnNbO_4$, and Zn_2TiO_4, J. Solid State Chem. **113**, 413 (1994).

[66] H. Kawai, M. Tabuchi, M. Nagata, H. Tukamoto, and A. R. West, Crystal chemistry and physical properties of complex lithium spinels $Li_2MM'_3O_8$ (M=Mg, Co, Ni, Zn; M′=Ti, Ge), J. Mater. Chem. **8**, 1273 (1998).

[67] K. Hirota, M. Ohtani, N. Mochida, and A. Ohtsuka, Formation and structure of spinel solid solution in Li_2O-MO-GeO_2 (M=Zn, Co, Ni) system, J. Ceram. Soc. Jpn. **96**, 92 (1988).

[68] M. Isobe and Y. Ueda, Observation of phase transition from metal to spin-singlet insulator in $MgTi_2O_4$ with S=1/2 Pyrochlore Lattice, J. Phys. Soc. Jpn. **71**, 1848 (2002).

[69] M. Schmidt, W. Ratcliff, P. G. Radaelli, K. Refson, N. M. Harrison, and S. W. Cheong, Spin singlet formation in $MgTi_2O_4$: Evidence of a helical dimerization pattern, Phys. Rev. Lett. **92**, 056402 (2004).

[70] W. B. St. Senz and D. Hesse, The effect of stress on cubic-to-tetragonal phase transitions in Mg_2TiO_4 and Mg_2GeO_4 spinel films, Philos. Mag. A **81**, 109 (2001).

[71] T. Yang, W.-G. Li, Q.-J. Liu, and Z.-T. Liu, Geometrical, elastic, electronic, phonon, and optical properties of Na_3AgO_2 from first-principles calculation, J. Phys. Chem. Solids **194**, 112210 (2024).

[72] M. Sofin, K. Friese, J. Nuss, E. M. Peters, and M. Jansen, Synthesis and crystal structure of Rb_3AgO_2, Z. Anorg. Allg. Chem. **628**, 2500 (2002).

[73] A.-V. Mudring and M. Jansen, Synthese und kristallstruktur von Cs_3AuO_2, Z. Anorg. Allg. Chem. **627**, 77 (2001).

[74] B. Darriet, M. Devalette, and B. Lecart, Détermination de la structure cristalline de K_3AgO_2, Rev. Chim. Miner. **14**, 423 (1977).